Chemical Communications

Dynamic Article Links ►

Cite this: DOI: 10.1039/c0xx00000x

www.rsc.org/xxxxxx

ARTICLE TYPE

Flexible, low-temperature, solution processed ZnO-based perovskite solid state solar cells

Mulmudi Hemant Kumar[1,2*], Natalia Yantara[1, 2*], Sabba Dharani[1,2], Michael Graetzel[3], Subodh Mhaisalkar[1, 2], Pablo. P. Boix[1#], Nripan Mathews[1, 2, 4#]

Received (in XXX, XXX) Xth XXXXXXXXX 20XX, Accepted Xth XXXXXXXXX 20XX

DOI: 10.1039/b000000x

A ZnO compact layer formed by electrodepositon and ZnO nanorods grown by chemical bath deposition (CBD) allow the processing of low-temperature, solution based and flexible solid state perovskite $CH_3NH_3PbI_3$ solar cells. Conversion efficiencies of 8.90 % were achieved on rigid substrates while the flexible ones yielded 2.62 %.

Solid-state organic-inorganic perovskite $(CH_3NH_3)PbX_3$ (X =Cl, Br, I) based nanostructured solar cells have recently gained a lot of attention due to their superior performance and ease of fabrication.[1-9] A power conversion efficiency of ~ 17 % has been identified as a realistic target, considering a short-circuit photocurrent density of 22 $mAcm^{-2}$ (based on a 1.5 eV bandgap), a photovoltage of 1.1 V and a fill factor of 0.7.[10] At the lab scale, power conversion efficiencies of 15 % have already been achieved utilizing a solution based two-step method to deposit the perovskite.[1] Now that it has been shown conclusively that the $CH_3NH_3PbX_3$ perovskite layers can form highly efficient solar cells, efforts must be focused on technologically relevant challenges.

Although the high efficiencies achieved are commendable, a cost effective low cost roll-to-roll production of solid state devices is only possible when the processing temperatures are brought down to 100-150 ^oC.[11-13] A low temperature approach can have other interesting advantages such as the fabrication of flexible devices, due to the instability of plastic substrates at high temperatures. Efforts have been made to lower the processing temperature of the porous metal oxide film. In this regard, Al_2O_3 was successfully employed as scaffold for the perovskite absorbing layer with an annealing temperature as low as 150 ^oC and a conversion efficiency of 12.3 % was obtained.[14] Nevertheless, the TiO_2 compact layer used between the conducting substrate and the scaffold (Al_2O_3) requires high temperature sintering at 450-500 ^0C,[14, 15] making it incompatible with plastic substrates. In the context of dye-sensitized solar cells, low temperature electrophoretic deposition has been widely employed to fabricate mesoporous TiO_2 and nano-porous ZnO on flexible indium-tin oxide (ITO) coated poly (ethylene terephthalate) (PET).[12, 13, 16] Other methods include anodization of sputtered titanium film for obtaining nanotubes directly on Kapton HN substrate, but high temperature annealing was again necessary to obtain reasonable efficiencies (3.5%).[17] More recently, Snaith et al have developed a high electron mobility TiO_2 mesoporous single crystal approach, which in combination with a spuncoated blocking layer yielded efficiencies of 7.28% with the perovskite absorber.[18]

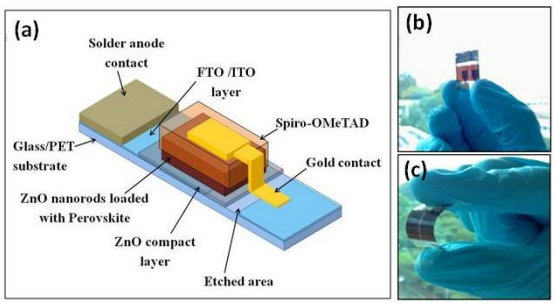

Figure 1. (a) Schematic illustration of the architecture for the perovskite devices fabricated in this work, (b) device on FTO substrate, and (c) device on flexible PET/ITO substrate.

ZnO is a viable alternative to TiO_2 for these classes of solar cells due to their comparable energy levels as well as good electron transport properties.[19-21] The feasibility of electrodepositing ZnO raises the possibility of eliminating the high temperature processed TiO_2 compact layer.[22-24] It has already been demonstrated that growing ZnO nanorods by chemical bath deposition (CBD) on electrodeposited ZnO can lead to both electrical and optical enhancements.[23] Here, we demonstrate complete low temperature processed (<100 ^oC) highly efficient perovskite solar cells with performance superseding previous reports.[18] By utilizing electrodeposited ZnO as compact layer and CBD grown nanorods, we extend this process to flexible devices as well resulting in promising performance.

The device configuration is presented in Figure 1(a). The ZnO nanorod film which acts as the electron transporting material and scaffold for the deposition of mesoscopic perovskite is grown on top of the ZnO compact layer. The compact layer functions as a hole blocking layer, preventing the recombination of electrons in FTO/ITO with the holes in spiro-MeOTAD. The planar (compact) ZnO film consists of angular grains which vary between 50-200 nm (Figure. 2(a)). This morphology is typical of such films as presented in previous reports.[24] The typical diameters of the ZnO nanorods grown on the ZnO film are in the range of 100-150 nm and the lengths were between 400-500 nm (Figure 2(d)). The difference in the morphology between these substrates has a direct impact on the loading of PbI_2 (Figure S2), where the increased loading of PbI_2 on the nanorods is evident. The poorer loading of PbI_2 on the planar ZnO translates to a less homogeneous structure when it is converted into the perovskite. This is confirmed by Figure 2 (b) & (e) which represents the cross-section of the perovskite islands on the ZnO planar layers

as well as on the ZnO nanorod sample. It is clear from the SEM images that the perovskite islands are bigger in size perpendicular to the ZnO planar substrate as compared to the nanorod sample. Similar substrate dependence on perovskite island formation has been shown previously.[1, 6]

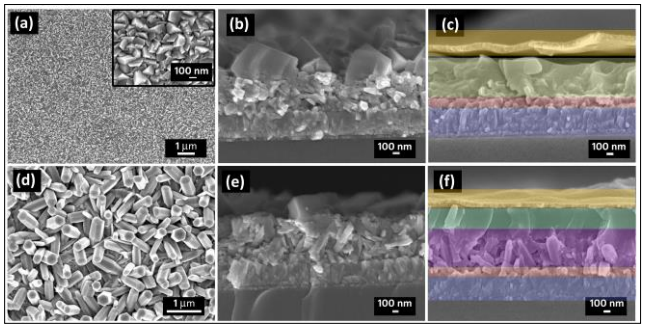

Figure 2. FESEM images of (a) top view of ZnO compact layer electrodeposited on FTO (inset shows high resolution image), (b) cross-section view of perovskite islands on ZnO compact layer, (c) cross-section view of the complete planar ZnO device; FTO (blue), ZnO BL (red), perovskite + spiro (light green), gold (yellow) (d) top view of ZnO nanorods grown on ZnO compact layer on FTO, (e) cross-section view of perovskite islands on ZnO nanorods, and (f) cross-section view of the complete ZnO nanorod device; FTO (blue), ZnO BL (red), ZnO nanorod + perovskite (purple), spiro (green), gold (yellow).

As the perovskite overlayer on planar devices was found to be thicker (and rougher) compared to the one on the nanorod samples, the optimum spiro-OMeTAD concentration used for nanorod sample was lower (90 mg/ml) compared to planar devices (120 mg/ml). The cross-section of the full device fabricated on FTO is shown in Figure 2 (c) & (f). Similar procedures were followed for the fabrication of perovskite solar cells on flexible substrates (PET/ITO). Details on the physical characterization of the ZnO compact layer on PET/ ITO are presented in the supporting information (Figure S1). Figure S3 (a) & (b) depicts the top view of the ZnO compact layer and the ZnO nanorods on PET/ITO substrate. It is interesting to note that solar cells fabricated with both planar and nanorods on flexible substrates yielded better performance with 120mg/ml of spiro-OMeTAD. This could be again attributed to a less homogeneous perovskite overlayer on these substrates.

Photovoltaic characteristics (j-V plots) of the devices fabricated on FTO and PET/ITO are presented in Figure 3(a). The photovoltaic parameters obtained are tabulated in Table 1. The performance of the devices fabricated on FTO in general supersedes the devices fabricated on PET/ITO, which is attributed to the inherent sheet resistance of the substrates used. However, the nanorod device (J_{sc} = 16.98 mAcm^{-2}, V_{oc} = 1.02 V, FF = 51.11 %, η = 8.90 %) demonstrates higher conversion efficiency than the planar device (J_{sc} = 11.27 mAcm^{-2}, V_{oc} = 1.08 V, FF = 45.44 %, η = 5.54 %) on FTO. The less irregular perovskite overlayer permits a thinner spiro-OMeTAD overlayer on the nanorod sample and this effect is reflected in the measured fill factors. FTO-nanorod based device has a fill factor of 51.11 % compared to the FTO-planar which has a fill factor of 45.44 %. Such an improvement of the nanorod device compared to the planar device is also observed for the PET/ITO substrates. However, the inherent high sheet resistance (60 Ω/sq) of PET/ITO plays a detrimental role. Other effects of the high sheet resistance could be non-uniformity in the electrodeposited ZnO blocking layer, which leads to lower dark current onset and consequently lower Voc for the PET/ITO substrates. Despite the differences in the substrates, the V_{oc} of the ZnO nanorod devices are lower compared to the planar devices where bulk of the electron transport occurs within the perovskite. This is similar to previous reports where ZrO_2 and Al_2O_3 were used as non-injecting scaffold layer and electron transport occurred within the perovskite. [14, 25] The photovoltaic parameters (J_{sc}, V_{oc}) as a function of light intensity are shown in Figure S4. A linear relationship of the current density versus light intensity indicate that collection efficiency is independent of light intensity, ruling out space-charge effects .[25]

The J_{sc} of the nanorod devices is enhanced which could be attributed to increased perovskite loading or/and increased charge collection. The observed effect is validated by the IPCE action spectra shown in Figure 3(b). The J_{sc} calculated from the IPCE data correlates with the J_{sc} calculated from the j-V plots, tabulated in Table 1. The shape of the IPCE spectrum for devices on FTO substrate is in agreement with the shapes reported in the literature as well.[1] However, there is a slight discrepancy with the shape of IPCE spectrum for devices on flexible PET/ITO substrates in the wavelength region of 400-600 nm as seen in Figure 3(b). This discrepancy in shape can be understood by considering the transmittance data of ZnO on various substrates plotted in Figure 3(c). As seen, the transmittance for both planar and nanorod ZnO sample on the PET/ITO decreases by ~ 30 % (at λ = 500 nm) compared to the ZnO on FTO substrate. Due to this reason, the IPCE is limited at shorter wavelengths (λ = 400-600 nm) for the flexible PET/ITO devices. Diffuse transmittance measurement (Figure S5) on the ZnO substrate alone proves that nanorod morphology increases the light scattering in both FTO and flexible PET/ITO substrate. Hence, the J_{sc} increment for the nanorod morphology can be attributed to better charge generation and collection efficiency due to increased light scattering and a larger heterojunction interface. The charge collection efficiency of the ZnO nanorods is clearly seen in the FTO nanorod device which achieves high APCE values of over 90 % at shorter wavelengths; see Figure 3(d).

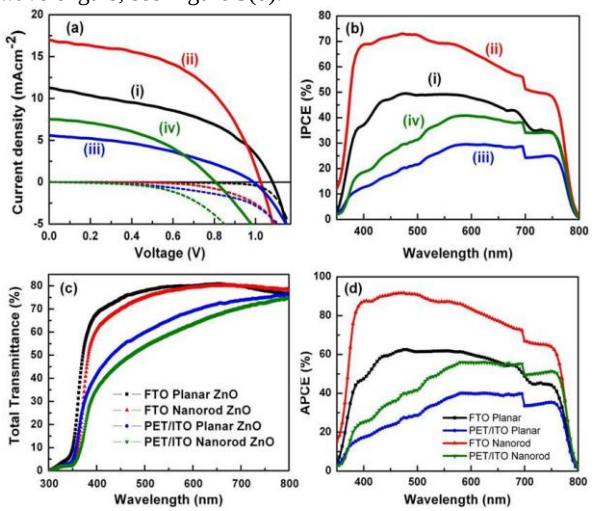

Figure 3. (a) j-V plots of (i) FTO planar device, (ii) FTO nanorod device (iii) PET/ITO planar device, (iv) PET/ITO nanorod device; (b) IPCE action spectra of (i) FTO planar device, (ii) FTO nanorod device (iii) PET/ITO planar device, (iv) PET/ITO nanorod device; (c) Total transmittance measured using integrating sphere, (d) Absorbed photon-to-current conversion efficiency (APCE) for the devices.

Nanorods-based devices systematically present lower V_{oc} than the planar ones, regardless of the higher charge generation as seen in the short circuit currents measured. In order to elucidate this loss in voltage, impedance spectroscopy was measured for both nanorods and planar devices on FTO under white LED illumination. The intensity of the white LED illumination was tuned so that the obtained J_{sc} in the devices matched the one obtained under AM1.5G illumination. Interestingly, the measured

spectra were described by a single arc and a lower frequency feature as seen in Figure 4(a), in contrast to previous reports on TiO_2 based devices [26-28] which featured additional components. The recombination resistance extracted from the fitting of the arc (Figure 4 (b)) shows higher recombination in the nanorod-based devices, which justifies the difference in V_{oc}. This increased recombination could occur due to the higher interfacial area.

Table 1. Photovoltaic parameters of devices fabricated in this study.

Device	J_{sc} ($mAcm^{-2}$)	V_{oc} (V)	FF (%)	η (%)	J_{sc} from IPCE ($mAcm^{-2}$)
FTO-Planar	11.27	1.08	45.44	5.54	10.90
FTO-Nanorod	16.98	1.02	51.11	8.90	15.70
PET/ITO-Planar	5.57	0.99	39.58	2.18	6.20
PET/ITO-Nanorod	7.52	0.80	43.14	2.62	8.60

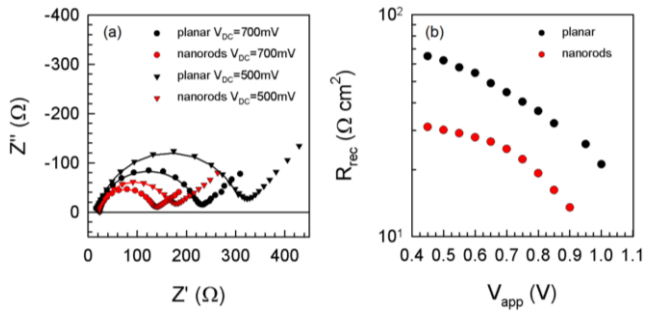

Figure 4. (a) Examples of Nyquist plots obtained from the IS measurement of planar and nanorods devices on FTO at different applied voltages under illumination (the solid lines correspond to the fitting) and (b) recombination resistance extracted from the fitting of the arc at lower frequencies.

We have demonstrated a simple yet potent methodology to fabricate a complete low temperature processed perovskite solid state solar cells. To the best of our knowledge, this is the foremost demonstration of perovskite solar cells employing ZnO compact layer as hole blocking layer and mesoscopic scaffold layer as an electron transporter. Remarkable power conversion efficiencies of 8.90 % were achieved on FTO based substrates and 2.62 % on flexible PET/ITO based substrates. Additionally, the present work indicates the suitability of low temperature planar ZnO as an underlayer for perovskite solar cells opening interesting possibilities. Increasing the amount of perovskite deposited on the planar layer and its homogeneity will therefore be a promising method to increase the efficiency.

We thank Mr. Julianto Chua and Ms. Pham Thi Thu Trang for valuable scientific discussions.

Notes and references

1. Energy Research Institute @NTU (ERI@N), Research Techno Plaza, X-Frontier Block, Level 5, 50 Nanyang Drive, Singapore 637553.
2. School of Materials Science and Engineering, Nanyang Technological University, Nanyang Avenue, Singapore 639798.
3. Laboratory of Photonics and Interfaces, EPFL, Lausanne, Switzerland.
4. Singapore-Berkeley Research Initiative for Sustainable Energy, 1 Create Way, Singapore 138602, Singapore.
** These authors contributed equally in this work.*
 # Correspondence to: PBPablo@ntu.edu.sg; Nripan@ntu.edu.sg

1. J. Burschka, N. Pellet, S.-J. Moon, R. Humphry-Baker, P. Gao, M. K. Nazeeruddin and M. Gratzel, *Nature*, 2013, **499**, 316-319.
2. E. Edri, S. Kirmayer, D. Cahen and G. Hodes, *Journal of Physical Chemistry Letters*, 2013, **4**, 897-902.
3. L. Etgar, P. Gao, Z. Xue, Q. Peng, A. K. Chandiran, B. Liu, M. K. Nazeeruddin and M. Grätzel, *Journal of the American Chemical Society*, 2012, **134**, 17396-17399.
4. J. H. Heo, S. H. Im, J. H. Noh, T. N. Mandal, C. S. Lim, J. A. Chang, Y. H. Lee, H. J. Kim, A. Sarkar, M. K. Nazeeruddin, M. Grätzel and S. I. Seok, *Nature Photonics*, 2013, **7**, 486-491.
5. J. H. Im, C. R. Lee, J. W. Lee, S. W. Park and N. G. Park, *Nanoscale*, 2011, **3**, 4088-4093.
6. J.-Y. Jeng, Y.-F. Chiang, M.-H. Lee, S.-R. Peng, T.-F. Guo, P. Chen and T.-C. Wen, *Advanced Materials*, 2013, **25**, 3727-3732.
7. H. S. Kim, C. R. Lee, J. H. Im, K. B. Lee, T. Moehl, A. Marchioro, S. J. Moon, R. Humphry-Baker, J. H. Yum, J. E. Moser, M. Grätzel and N. G. Park, *Scientific Reports*, 2012, **2**.
8. H. S. Kim, J. W. Lee, N. Yantara, P. P. Boix, S. A. Kulkarni, S. Mhaisalkar, M. Grätzel and N. G. Park, *Nano Letters*, 2013, **13**, 2412-2417.
9. A. Kojima, K. Teshima, Y. Shirai and T. Miyasaka, *Journal of the American Chemical Society*, 2009, **131**, 6050-6051.
10. N.-G. Park, *The Journal of Physical Chemistry Letters*, 2013, 2423-2429.
11. M. Durr, A. Schmid, M. Obermaier, S. Rosselli, A. Yasuda and G. Nelles, *Nat Mater*, 2005, **4**, 607-611.
12. T. Miyasaka and Y. Kijitori, *Journal of the Electrochemical Society*, 2004, **151**, A1767-A1773.
13. L. Grinis, S. Kotlyar, S. Rühie, J. Grinblat and A. Zaban, *Advanced Functional Materials*, 2010, **20**, 282-288.
14. J. M. Ball, M. M. Lee, A. Hey and H. J. Snaith, *Energy and Environmental Science*, 2013, **6**, 1739-1743.
15. M. J. Carnie, C. Charbonneau, M. L. Davies, J. Troughton, T. M. Watson, K. Wojciechowski, H. Snaith and D. A. Worsley, *Chemical Communications*, 2013, **49**, 7893-7895.
16. T. Yoshida, T. Oekermann, K. Okabe, D. Schlettwein, K. Funabiki and H. Minoura, *Electrochemistry*, 2002, **70**, 470-487.
17. A. Vomiero, V. Galstyan, A. Braga, I. Concina, M. Brisotto, E. Bontempi and G. Sberveglieri, *Energy & Environmental Science*, 2011, **4**, 3408-3413.
18. E. J. W. Crossland, N. Noel, V. Sivaram, T. Leijtens, J. A. Alexander-Webber and H. J. Snaith, *Nature*, 2013, **495**, 215-219.
19. Q. Zhang, C. S. Dandeneau, X. Zhou and C. Cao, *Advanced Materials*, 2009, **21**, 4087-4108.
20. J. B. Baxter and E. S. Aydil, *Applied Physics Letters*, 2005, **86**, 1-3.
21. I. Gonzalez-Valls and M. Lira-Cantu, *Energy and Environmental Science*, 2009, **2**, 19-34.
22. S. Otani, J. Katayama, H. Umemoto and M. Matsuoka, *Journal of the Electrochemical Society*, 2006, **153**, C551-C556.
23. N. Yantara, N. Mathews, K. B. Jinesh, H. K. Mulmudi and S. G. Mhaisalkar, *Electrochimica Acta*, 2012, **85**, 486-491.
24. M. Izaki and T. Omi, *Journal of the Electrochemical Society*, 1997, **144**, 1949-1952.
25. D. Bi, S.-J. Moon, L. Haggman, G. Boschloo, L. Yang, E. M. J. Johansson, M. K. Nazeeruddin, M. Gratzel and A. Hagfeldt, *RSC Advances*, 2013, **3**, 18762-18766.
26. H.-S. Kim, C.-R. Lee, J.-H. Im, K.-B. Lee, T. Moehl, A. Marchioro, S.-J. Moon, R. Humphry-Baker, J.-H. Yum, J. E. Moser, M. Grätzel and N.-G. Park, *Scientific Reports*, 2012, **2**, 1-7.
27. H.-S. Kim, J.-W. Lee, N. Yantara, P. P. Boix, S. A. Kulkarni, S. Mhaisalkar, M. Grätzel and N.-G. Park, *Nano Letters*, 2013, **13**, 2412-2417.
28. H.-s. Kim, I. Mora-Sero, V. Gonzalez-Pedro, F. Fabregat-Santiago, E. J. Juarez-Perez, N.-g. Park and J. Bisquert, *Nature communications*, 2013, **4**, 1-7.